Sahba Mobini, Masoud Taghizadeh-Jahed, Manijeh Khanmohammadi, Ali Moshiri, Mohammad-Mehdi Naderi, Hamed Heidari-Vala, Javad Ashrafi Helan, Sayeh Khanjani, Armin Springer, Mohammad-Mehdi Akhondi, Somaieh Kazemnejad

Comparative evaluation of in vivo biocompatibility and biodegradability of regenerated silk scaffolds reinforced with/without natural silk fibers

Erstveröffentlichung in / First published in:

Journal of Biomaterials Applications. 2016, 30(6), S. 793 - 809 *[Zugriff am: 15.08.2019]*. SAGE journals. ISSN 1530-8022.

DOI: https://doi.org/10.1177/0885328215601925

JOURNAL OF
biomaterials applications

Original Article

Journal of Biomaterials Applications
2016, Vol. 30(6) 793–809

DOI: 10.1177/0885328215601925
jba.sagepub.com
SAGE

Comparative evaluation of *in vivo* biocompatibility and biodegradability of regenerated silk scaffolds reinforced with/without natural silk fibers

Sahba Mobini[1], Masoud Taghizadeh-Jahed[1], Manijeh Khanmohammadi[1], Ali Moshiri[1], Mohammad-Mehdi Naderi[1], Hamed Heidari-Vala[1], Javad Ashrafi Helan[2], Sayeh Khanjani[1], Armin Springer[3], Mohammad-Mehdi Akhondi[1] and Somaieh Kazemnejad[1]

Abstract

Nowadays, exceptional advantages of silk fibroin over synthetic and natural polymers have impelled the scientists to application of this biomaterial for tissue engineering purposes. Recently, we showed that embedding natural degummed silk fibers in regenerated *Bombyx mori* silk-based scaffold significantly increases the mechanical stiffness, while the porosity of the scaffolds remains the same. In the present study, we evaluated degradation rate, biocompatibility and regenerative properties of the regenerated 2% and 4% wt silk-based composite scaffolds with or without embedded natural degummed silk fibers within 90 days in both athymic nude and wild-type C57BL/6 mice through subcutaneous implantation. In all scaffolds, a suitable interconnected porous structure for cell penetration was seen under scanning electron microscopy. Compressive tests revealed a functional relationship between fiber reinforcement and compressive modulus. In addition, the fiber/fibroin composite scaffolds support cell attachment and proliferation. On days 30 to 90 after subcutaneous implantation, the retrieved tissues were examined via gross morphology, histopathology, immunofluorescence staining and reverse transcription-polymerase chain reaction as shown in Figure 1. Results showed that embedding the silk fibers within the matrix enhances the biodegradability of the matrix resulting in replacement of the composite scaffolds with the fresh connective tissue. Fortification of the composites with degummed fibers not only regulates the degradation profile but also increases the mechanical performance of the scaffolds. This report also confirmed that pore size and structure play an important role in the degradation rate. In conclusion, the findings of the present study narrate key role of additional surface area in improving *in vitro* and *in vivo* biological properties of the scaffolds and suggest the potential ability of these fabricated composite scaffolds for connective tissue regeneration.

Keywords

Silk fibroin, fiber-reinforced composites, biodegradability, biocompatibility, tissue engineering

Introduction

Healing and regeneration of large connective tissue defects are major challenge in trauma surgery.[1,2] The current procedures using autografts and allografts are associated with significant limitations and complications such as the need for multiple surgeries, additional surgical time/cost, donor-site morbidity and limited supply in overly large defects. Tissue engineering and regenerative medicine (TERM) approaches that deliver scaffolds, cells and growth factors directly into

[1]Department of Tissue Engineering, Reproductive Biotechnology Research Center, Avicenna Research Institute, ACECR, Tehran, Iran
[2]Department of Pathology, Faculty of Veterinary Medicine, University of Tabriz, Tabriz, Iran
[3]Centre for Translational Bone, Joint and Soft Tissue Research, University Hospital Carl Gustav Carus and Medical Faculty of Technische Universität Dresden, Dresden, Germany

Corresponding author:
Somaieh Kazemnejad, Department of Tissue Engineering, Reproductive Biotechnology Research Center, Avicenna Research Institute, P.O. Box: 19615-1177 Tehran, Iran.
Email: s.kazemnejad@avicenna.ac.ir; kazemnejad_s@yahoo.com

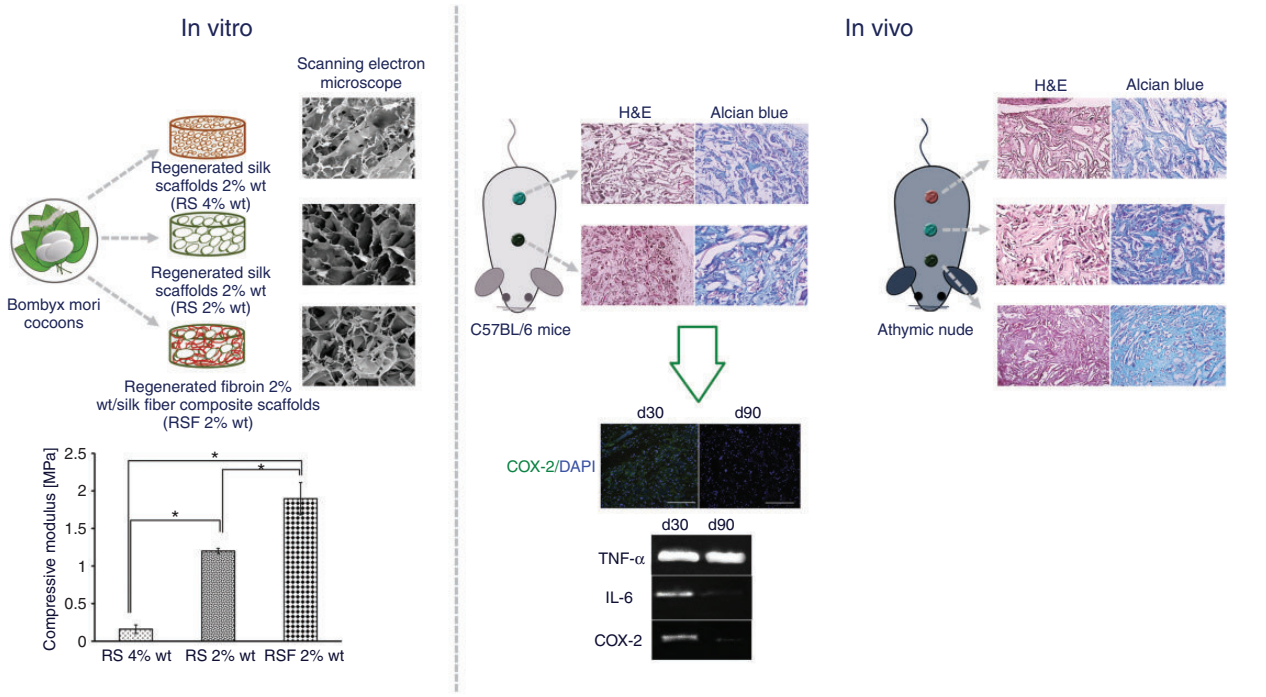

Figure 1. Illustrative summary of the main methods and findings.
RS: regenerated silk; RSF: regenerated fibroin/ silk fiber composite scaffolds; H&E: Hematoxylin and eosin; COX-1: Cyclooxygenase.

affected defects hold great potential for achieving optimal healing in these difficult cases, while eliminating the drawbacks related to conventional treatments.[3,4] Scaffolds as main components of fabricated constructs should be able to substitute the missing part of the targeted tissue and boost its regeneration. In addition, these structures should have suitable biocompatibility, biodegradability, appropriate mechanical properties and desired bioactivity.[5] Nowadays, the scientists have been fascinated by silk biomaterials due to exceptional advantages of silk fibroin over synthetic and natural polymers. Low immunogenicity, cell affinity, modifiable degradation rates and impressive mechanical properties make silk as a promising candidate for TERM goals.[6–8] Nevertheless, variety of silk scaffolds can be developed from aqueous to solvent formulations of the natural fiber for utilizing in different targets.[9–11]

Actually appropriate degradation rate is an essential requirement for biocompatibility of an engineered cell-scaffold construct. Suitable degradation rate consistent with the new tissue ingrowths results in the mechanical and structural integrity with surrounding host tissue.[12,13] Although natural unprocessed silk as an FDA-approved biomaterial has been introduced as non-biodegradable material, according to the literature, silk fibroin is classified as enzymatically degradable polymer.[14] *In vitro* and *in vivo* studies revealed that silk fibroin degradation behavior is highly influenced by structural characterization, original preparation methods, solvent, porosity and morphology of scaffold and host immune system elements during degradation.[15,16] Therefore, modification in physical form and post-treatment of silk biomaterials may allow tuning rate of degradation.

Recently, to construct an appropriate scaffold for osteochondral tissue engineering, a novel *Bombyx mori* silk-based composite scaffold was fabricated by embedding the natural degummed silk fibers within a matrix of regenerated fibroin for tissue engineering purpose. These highly porous scaffolds hold more compressive modulus compared to regenerated fibroin without natural silk fibers with the same porosity.[17] However, *in vivo* biocompatibility and biodegradability of this modified composite scaffold remained to be assessed. In the present study, we examined *in vivo* degradation rate and biocompatibility of the 2% and 4% wt regenerated silk-based composite scaffolds with or without embedded natural degummed silk fibers in animal model. Because ''subcutaneous implantation'' is assumed to be a suitable model for evaluation of biodegradation,[16–19] the scaffolds were implanted subcutaneously and examined within 90 days in both athymic nude and wild-type C57BL/6 mice via histopathology, immunofluorescence staining and reverse transcription-polymerase chain reaction (RT-PCR).

As a main goal, we evaluated the role of silk fibers and regenerated fibroin concentration in the biodegradation behavior and regenerative capacity of the composite scaffolds composed of regenerated fibroin matrix/natural silk fibers.

Materials and methods

Ethics

The investigators who undertook the measurements and analyses of the results were unaware of the experimental design and grouping details. All operative procedures were performed by one surgeon. All animals received human care in compliance with the Guide for Care and use of Laboratory Animals published by the National Institutes of Health (NIH publication no. 85-23, revised 1985). The study was approved by bioethic committee of Avicenna Research Institute.

Preparation of silk fibroin scaffolds

Silk fibroin was extracted from *Bombyx mori* silkworm cocoons (Provided by Iranian silkworm Research Center; Guilan, Iran) according to the procedures described in our previous studies.[17,20] Briefly, three cocoons were boiled for 1 h in 750 mL of 0.02 M Na_2CO_3 (Merck, Darmstadt, Germany) solution, rinsed with deionized water and dried overnight. The dried and degummed fibers containing water-insoluble fibroin were dissolved in 9.3 M LiBr (Merck, Darmstadt, Germany) solution (10 wt% fibers) for 5 h at 55°C and dialyzed with cellulose dialysis tubes (12 KDa cut-off value) (Sigma Aldrich, Taufkirchen, Germany) against ultra-pure water for 36 h. The fibroin solution was freeze-dried to allow storage of the extracted fibroin at room temperature (RT).

For preparation of the regenerated silk (RS) scaffolds, the lyophilized fibroin was dissolved in ultrapure water to a final concentration of 2 and 4% wt, respectively. The scaffolds were fabricated in disc-shaped matrices (3 × 4 mm) by pouring 140 µL of the fibroin solution per well into 96-well tissue culture polystyrene plates (TTP, Trasadingen, Switzerland). Then, the scaffolds were freeze-dried to generate porous matrix, which were then treated with 99.98% methanol (Merck, Darmstadt, Germany) for 1 h to regenerate β-sheet domains. Finally, to eliminate the methanol, the scaffolds were rinsed and freeze-dried, again.

Regenerated fibroin/silk fiber composite scaffolds (RSF) consisting of natural degummed silk fibers and regenerated fibroin were fabricated in disc shape as fully described in our previous work.[17] Degummed silk fibers were filled into 96-well tissue culture polystyrene plates. At fibers top, 140 µL of the 2 % wt fibroin solution was slowly poured to reach a mass ratio of silk fiber per dry fibroin as 10:4. In a similar manner with RS scaffolds, the RSF scaffolds were frozen, freeze-dried and treated with methanol (99.98%) in order to restore the β-sheet structure of the fibroin matrix.

Characterization of the fabricated scaffolds

Extracted fibroin protein was analyzed by Fourier transform infrared spectroscopy (FT-IR) pre-and post-methanol treatment using 55FTIR EQUINOX spectrophotometer (BrukerOptik GmbH, Ettlingen, Germany). Freeze-dried fibroin was mixed with KBr and precipitated. The pellets were analyzed in the range of 4000 to 500 cm^{-1} with a resolution of 4 cm^{-1}. To determine the conformation of both the methanol-treated and non-treated SF scaffolds, they were manually crushed to a fine powder by agate mortar. X-ray scans were performed by a SIEMENS D5000 diffractometer (Siemens, Munich, Germany) at 40 kV and 40 mA. All scans were extended from 5 to 70° in 2θ using Cu-Kα radiation.

After samples were gold coated using a sputter coater, the morphology of the fibers was characterized using a scanning electron microscope (SEM, Model XL30; Philips Electron Optics, Eindhoven, the Netherlands). Diameter of the fibers was measured from the provided SEM images using image analysis software.

Moreover, mechanical properties of the scaffolds (n = 6) were measured using an Instron 5566 testing machine (InstronWolpert GmbH, Pfungstadt, Germany) equipped with a 100 N load cell at ambient temperature. The crosshead speed was set at 1 mm min^{-1} for static uniaxial loading compression experiment. Cylinder-shaped samples measuring between 6.5 and 8 mm in diameter and ranging 9–13 mm in height were used, according to the modified ASTM method F451-95.[21–23] The samples were prepared using razor blades in dry condition and the compressive stress and strain were (elastic modulus) determined as previously described.[17]

In vitro cytocompatibility of scaffolds

To assess *in vitro* cytocompatibility of the prepared scaffolds, the morphology of human bone marrow-derived mesenchymal stem cells (hBMSCs) grown on the scaffolds was studied 21 days post cell seeding by SEM. Briefly, the hBMSCs were isolated from bone marrow aspirates (5–10 mL) using a combination of density gradient centrifugation and plastic adherence as described in our previous studies.[24] Before cell seeding, the disc-shaped scaffolds were sterilized by Gama-irradiation (30–35 kGy) and then immersed in

Dulbecco's modified Eagle's medium (DMEM)-low glucose overnight. The bone marrow-derived mesenchymal stem cells (BMSCs) grown in cell culture flasks were trypsinized, counted and plated at a density of 1.2×10^5 cells/cm^2 onto the surface of prepared scaffolds. Cellular scaffolds were incubated at 37°C for 1 h to allow BMSCs to diffuse into and adhere to the scaffold before the addition of 1 mL of medium to each well. The seeded cells on the scaffolds were cultured in DMEM-low glucose supplemented with 15% fetal bovine serum and 2 mM L-glutamine in a humid atmosphere of 5% CO_2 and 95% air at 37°C. At 14 and 21 days after cell seeding, the cell–scaffold constructs were rinsed twice with phosphate-buffered saline (PBS) and fixed in 2.5% glutaraldehyde for 2 h. The scaffolds were further rinsed with PBS and fixed in 1% Osmium Tetroxide for 1.5 h. After washing with PBS, samples were dehydrated with increasing concentrations of ethanol (50%, 70%, 90% and 100%) for 20 min each. Thereafter, the cell–scaffold constructs were air-dried overnight. After drying, the scaffolds were mounted on aluminum stubs and coated with gold–palladium (AuPd). Finally, surfaces of the various specimens were analyzed by Philips XL 30/ESEM (Philips, Eindhoven, The Netherlands).

In vivo implantation of silk-based scaffolds

To obtain the information regarding biodegradability, biocompatibility and regenerative properties of the silk-based scaffolds (RS 2 and 4% wt and RSF 2% wt), *in vivo* subcutaneous implantation test was accomplished in three time points in both male athymic nude and C57BL/6 mice (weighing 20–25 g). The animals were anesthetized by intramuscular administration of Ketamine HCL (50 mg/kg) and Xylazine HCL (5 mg/kg). Under aseptic condition, six longitudinal skin incisions (5 mm length) were made on the dorsum back of three athymic nude mice and the disk-shaped (3×4 mm) RS 2% wt ($n = 2$) and 4% wt ($n = 2$) and RSF 2% wt ($n = 2$) scaffolds were implanted subcutaneously in each animal (totally six scaffolds in each). Based on the *in vivo* results obtained from implantation of the scaffolds in nude mice, the RS ($n = 9$) and RSF ($n = 9$) 2% wt scaffolds were selected and implanted in another nine C57BL/6 mice so that in each animal two types of scaffolds (RS 2%: $n = 1$; RSF 2% $n = 1$) were implanted subcutaneously on the dorsum back. Skin incisions were approximated by metal clips. Postoperative analgesia and antibiotic were provided by intramuscular administration of Tramadol (10 mg/kg) twice a day for three days and Gentamicin (10 mg/kg) daily for five days, respectively. After induction of short-time anesthesia, the wound clips were removed seven days later. Then, the animals were euthanized to retrieve the scaffolds for analysis 30, 60 and 90 days after implantation. Nude mice were considered as external control for C57BL/6 mice while in each animal, each scaffold was considered as internal control for the other scaffold/s.

Sample collection

In each time point, totally 36 scaffolds in 12 mice were evaluated. Half of the scaffolds were dissected from nude mice, while another half was dissected from C57BL/6 mice. For gross morphology, all the scaffolds were evaluated. Each scaffold was sectioned and divided into two parts. The first part was used for histopathologic and fluorescent microscopic evaluations, while another part was used for RT-PCR analyses.

Gross and histopathologic examinations

For gross pathology, the hyperemia, development and quality of the capsule, biodegradability and other gross characteristics were qualitatively evaluated and reported by two expert comparative healing pathologists. Immediately after euthanasia, the remained parts of the implanted scaffolds together with the covering newly regenerated tissues were harvested, collected and fixed in buffered formalin (10%) for at least 24 h. Then the samples were dehydrated in a graded series of ethanol, cleared in xylene, embedded in paraffin wax, sectioned at 4–5 μm, and stained with either the Hematoxylin and eosin (H & E) and Alcian blue and nuclear fast red (AB-NFR).The stained slides were evaluated under a light microscope (Olympus BX51, Tokyo, Japan) connected to a digital camera (Olympus DP71) by two expert pathologists. In each group of scaffolds, five histopathologic fields (×100) were used for semi-quantitative analyses. The percentage of filled pores with the newly regenerated tissue per total pores, number of the remained pores inside the scaffold, total cellularity, fibroblast, fibrocyte, neutrophil, lymphocyte, macrophage, total vascularity and small-, medium- and large sized vessels were counted at triplicate. The counting was performed by software (Photoshop CC, ADOBE Corp., CA and Image J, NIH, CA).

For immunohistochemical staining of Cyclooxygenase-2 (COX-2), non-specific binding sites on the sections were blocked with 10% goat serum in PBS and incubated with COX-2 polyclonal antibody (1:200) (Thermo scientific Inc. Waltham, MA) and secondary FITC-conjugated goat anti-rabbit Ig (1:200) (Abcam, Cambridge, London). All the sections were counterstained with DAPI (4, 6-diamidino-2-phenylindole; 1:1000) (Sigma Aldrich Co. LLC.USA) for nuclear staining. The tissue samples were visualized

Table 1. Sequences of the primers used for analysis of inflammation-related genes in sample tissues.

Name of gene	Primer sequence	Product size (bp)	NCBI accession number
TNF-α	F 5′-CCCAAAGGGATGAGAAGTTC-3′	245	NM_013693.3
	R 5′- GGAGTAGACAAGGTACAACC-3′		
COX-2	F 5′-CAGCACTTCACCCATCAGT-3′	181	NM_011198.3
	R 5′-GATACACCTCTCCACCAATG-3′		
IL-6	F 5′-CACGGCCTTCCCTACTTCAC-3′	186	NM_031168.1
	R 5′- GCAAGTGCATCATCGTTGT-3′		
TBP	F 5′- AAGGGAGAATCATGGACCAGAAC-3′	149	NM_013684.3
	R 5′-GGTGTTCTGAATAGGCTGTGGAG-3′		

TNF-α: Tumor necrosis factor-α; COX-2: cyclooxygenase-2; IL-6: interleukin-6; TBP: TATAA-box binding protein.

and photomicrographed using an epifluorescence microscope (Olympus BX51, Tokyo, Japan) connected to a digital camera (Olympus DP71).

RT-PCR

RT-PCR was performed to assess expression of a set of inflammation-related genes including interleukin-6 (IL-6), COX-2 and tumor necrosis factor-α (TNF-α) in the retrieved samples. Briefly, total RNA was extracted from tissue samples using RNeasy Mini Kit (Qiagen, Valencia, USA). Reverse transcription was performed using 2 μg purified RNA and SuperScript™ II Reverse Transcriptase kit (Gibco, New York, USA) in a thermocycler (Eppendorf, Germany). Then, 1 μL of cDNA was admixed with 12.5 μL reaction master mix (Amplicon, Copenhagen, Denmark) and 1 μL of each primer (Table 1). After initial denaturation at 95°C for 10 s, PCR amplification was continued at 95°C for 5 s and 60°C for 30 s for 40 cycles. Finally, dissociation stage was performed at 95°C for 15 s, 60°C for 1 min and 95°C for 15 s. The amplified DNA fragments were electrophoresed on 2% agarose gel and visualized by ultra-violet transilluminator (Uvitec, Cambridge, UK). Expression of each gene was corresponded to TATAA-box-binding protein (TBP) as an internal control. ***RAW264.7*** (Mouse leukemic monocyte macrophage cell line) (Eton Bioscience. Inc. San Diego, CA) was used as a positive control. For semi-quantitative determination, specific band density was normalized to that of the corresponding using AlphaEase software (Genetic Technologies, Inc., Fitzroy Vic 3065 Australia).

Statistical analyses

For multiple comparisons, One Way ANOVA with its subsequent post hoc Tukey tests was used, while for two comparisons the measured values were compared using Independent sample *t*-test. The results were expressed as mean ± standard deviation. A value of $P < 0.05$ was considered statistically significant.

Results

Physical and mechanical characteristics of the fabricated scaffolds

XRD and FT-IR analyses were carried out to characterize extracted fibroin before and after methanol treatment. Before methanol treatment, XRD results showed two strong peaks around $2\theta = 14$ and 16.5 representing silk I structure for extracted fibroin. After methanol treatment, the peaks shifted to $2\theta = 20$ and 21, respectively, indicating a conformation change from silk I to silk II with its crystalline β-sheet structure (Figure 2(a)). Protein characteristic peaks were found at different distinguishable vibration peak ranges relating to amide groups. Proteins showed characteristic vibration bands at 1650–1630 cm^{-1} for amide I (C = O stretching), 1540–1520 cm^{-1} for amide II (secondary NAH bending), and 1270–1230 cm^{-1} for amide III (CAN and NAH functionalities) in their FT-IR spectra. In Figure 2(b), peaks of fibroin before methanol treatment positioned at 1638, 1531 and 1242 cm^{-1} represent amides I, II and III, respectively. Moreover, the peak at 658 cm^{-1} was a validation for amide V. FT-IR revealed a silk I structure of the extracted fibroin. After methanol treatment, characteristic peaks at 1633, 1514 and 1235 cm^{-1} representing amides I, II and III, respectively, were found. The change of wave number of the vibration bands indicated the reorganization of hydrogen bonds due to the methanol treatment, characteristic for silk II formation.

During the mechanical assessment, none of the samples fractured. Compressive moduli (elastic modulus) of RS scaffolds rose with increasing fibroin concentration, starting at 0.16 MPa for RS 2 wt%, 1.20 MPa for RS 4% wt and reaching 13.97 MPa for RSF 2% wt, showing a high significant difference ($P = 0.001$) among

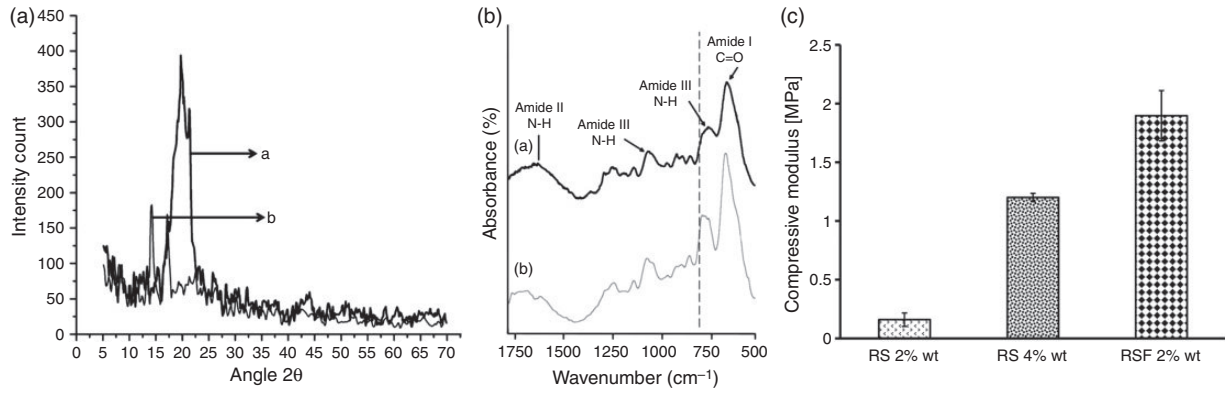

Figure 2. Physical and mechanical evaluations of silk-based scaffolds. A: XRD pattern of Silk fibroin (a) before regeneration (b) after regeneration with methanol. B: FTIR spectra of Silk fibroin (a) before regeneration (b) after regeneration with methanol. C: Compressive modulus of RS 2% wt, RS 4% wt and RSF 2% wt scaffolds in static dry condition. *indicates significant differences ($P \leq 0.05$) between groups.
RS: regenerated silk; RSF: regenerated fibroin/ silk fiber composite scaffolds.

each other. Thus, by adding fibers as reinforcing factor to the fibroin matrix, compressive moduli improved significantly more than 10 folds (Figure 2(c)).

Based on the SEM images, the RS showed a well porous structure as both the longitudinal, transverse sections of the scaffold were highly porous, and the pores were formed both on the surface and in the internal parts of the scaffold. Indeed, the pores were randomly but homogenously distributed all over the scaffold. By decrease in the concentration of RS matrix, the pore size significantly increased so that the RS 2% wt scaffolds had significantly larger pores (300 μm with median porosity of 90%) than those of the 4% wt ones (100 μm with mean porosity of 87%). RS with more than 4% wt concentration showed less pore size (<70 μm). The morphological assessment of RSF 2% wt scaffolds clearly showed that the fibers were embedded and randomly distributed all over the RS matrix. The mean pore size and porosity of RSF 2% were 200 μm and 88%, respectively. Image analyses of the SEM micrographs of the cell-seeded scaffolds exhibited that the cells penetrated and adhered on the surface of all the three scaffolds. Moreover, the cells expanded and distributed all over the scaffold surfaces during 21 days post cell seeding. As shown in Figure 3, the cell–cell interaction, proliferation and distribution over surfaces in RS 2% and RSF 2% wt is more significant than that of RS 4%. However, cells penetration is more typical in RSF 2% and RS 4% wt compared to RS 2% wt.

Gross pathology and histopathological findings

In nude mice. As shown in Figures 4 and 6, the RSF 2% wt scaffold architecture was not preserved and gradually degraded post-subcutaneous implantation. More connective tissue covered the RSF 2% wt scaffolds when compared to those of the RS 2% and 4% wt ones. In addition, the hyperemia was well developed and distributed all over the covering connective tissue of the RSF 2% wt scaffold, while in those of the RS 4% wt ones, the hyperemia was almost limited to the center of the connective tissue. RSF 2% wt scaffold triggered development of the fibrous connective tissue subcutaneously so that the developing tissue consisting of vascular structures and fibrous-like texture was well extended subcutaneously even outside the scaffold. This characteristic was not seen in other scaffolds.

Based on the qualitative and quantitative data obtained from H & E and Alcian Blue stained sections (Figures 4 and 6, Table 2), the RS 2% wt scaffolds were partially degraded during 90 days post-subcutaneous implantation in nude mice. On day 90, a few capsular tissues surrounded the scaffolds and a newly regenerated tissue evenly developed in situ. Unlike RS 2% wt, in the 4% wt one, a fibrous tissue well encapsulated the scaffold, one month post implantation. In this time, the scaffold was filled with the newly regenerated connective tissue consisting of fibroblast and collagenous tissue. Indeed, some sections of the RS 4% wt scaffold were infiltrated by the fibroblasts so that the cells proliferated and produced matrix and the newly regenerated tissue expanded and compressed the free pores. Interestingly, large blood vessels were formed inside the scaffold (RS 4% wt), at 90 days post implantation leading to an inflammatory reaction. In the case of RSF 2% wt scaffold, a well-organized connective tissue covered the scaffold 30 days post subcutaneous implantation so that it is well integrated with the newly developed connective tissue. The architecture of the pores and silk sheet was almost completely degraded

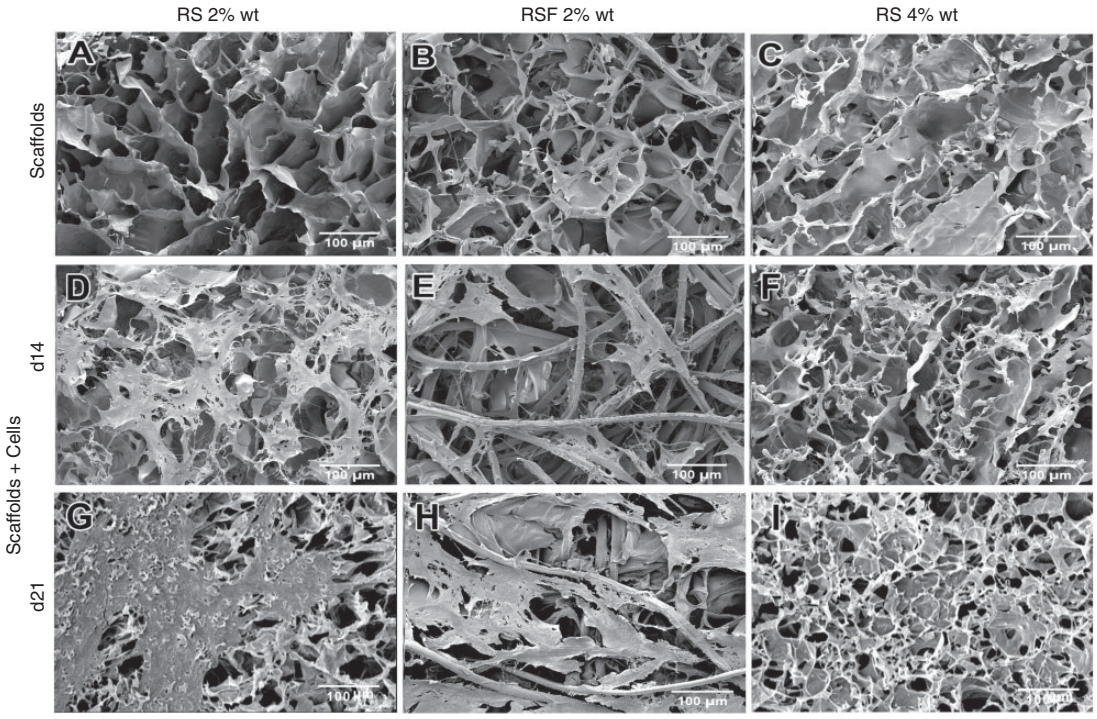

Figure 3. SEM images of the scaffolds structure. The structure of the RS 2% wt (A), RSF 2% wt (B) and RS 4% wt (C) without cell. The BMSCs morphology on the RS 2% wt (D, G), RSF 2% wt (E, H) and RS 4% wt (F, I) scaffolds after cultivation for 14 and 21 days, magnification 200×.
RS: regenerated silk; RSF: regenerated fibroin/ silk fiber composite scaffolds.

and replaced with the new connective tissue 30 days post implantation, while the natural silk fibers were present inside the scaffold at that time. Although the silk fibers of the RSF 2% wt scaffold remained in the nude mice even after 90 days, their transverse diameter slightly decreased as measured by software (ADOBE Photoshop CS-6. CA).

Ninety days post subcutaneous implantation, in the RSF 2% wt scaffolds, significantly higher number of pores were filled with the newly regenerated tissue ($P = 0.001$) and lower number of pores remained in the scaffolds compared to those of the RS 4% wt ones ($P = 0.001$). At this stage, the RSF 2% wt scaffolds had significantly higher fibroblast and fibrocyte compared to those observed in the RS 4% wt scaffolds ($P = 0.001$ for all) (Table 2). After 60 days post subcutaneous implantation of the RS 4% wt scaffold in nude mice, the architecture of the scaffold was completely preserved and was not degraded. The scaffold was surrounded by the capsular-like tissue and fibroblasts were laid between the matrices but the number of macrophages was higher than the fibroblasts. Thirty days later, the newly regenerated blood vessels were well developed inside the scaffold; however, at this stage, numerous lymphocytes and macrophages were infiltrated the scaffold. (Figure 4, Table 2).

In wild-type C57BL/6 mice. The assessment of biocompatibility and biodegradability of RS 2% wt and RSF 2% wt scaffolds was followed in wild-type C57BL/6 mice without immune suppression.

After subcutaneous implantation of the RS 2% wt and RSF 2% wt scaffolds in the C57BL/6 mice, different patterns of biocompatibility, biodegradability and regenerative capacity were seen in those of the RS 2% wt scaffolds when compared to their *in vivo* characteristics in nude mice (Figures 5 and 7). Unlike to those observed in nude mice, the RS 2% wt scaffolds were covered with a loose low thickness capsule in normal mice at day 30 post implantation. In addition, a number of inflammatory cells entered the scaffold and attached to its pores at that stage. After staining with Alcian blue-nuclear fast red, a better morphology of the cluster-like cells was seen and the structure of scaffold with the new matrix was better defined from each other. No evidence of connective tissue regeneration was evident 30 days post subcutaneous implantation of the scaffold. At 60 days post implantation, the internal architecture of the RS 2% wt scaffold was almost completely free of any cellular structures similar to that observed for the scaffold architecture before implantation. However, at this stage, the thickness of the capsule slightly increased and some blood vessels were evident in the covering capsule. In addition, a new

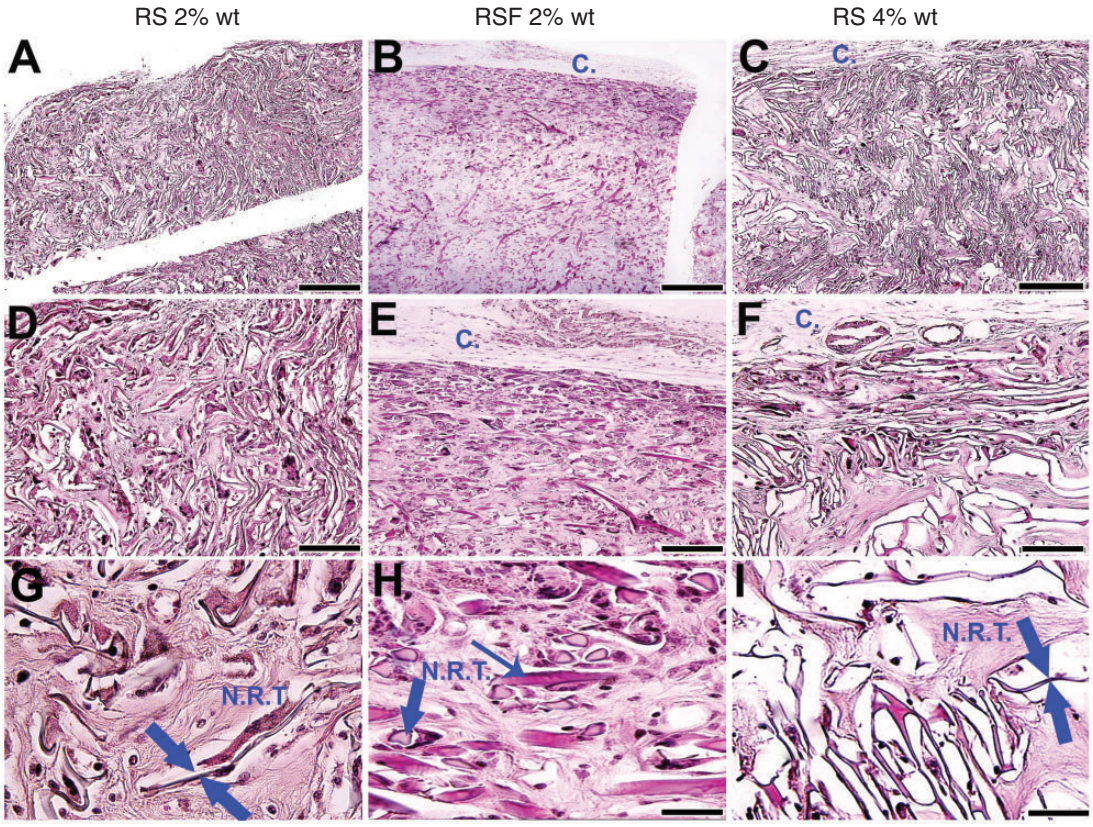

Figure 4. Histopathological appearance of different scaffolds, 90 days post subcutaneous implantation in athymic nude mice. The RS 2% wt scaffold has been partially degraded by the host (A, D, G) and a considerable part of it has been filled with the newly regenerated tissue (G; N.R.T). In addition, the architecture of the scaffold has been partially preserved and some remnants of the RS scaffold (G; arrow). A connective tissue like capsule (C.) has covered the RSF 2% wt scaffold (B, F). The regenerated matrix of the RSF 2% wt scaffold has been almost degraded by the host and replaced by the newly regenerated tissue (H; N.R.T.) but the natural fibers are present in the scaffold. These fibers have been sectioned both longitudinally (H; thin arrow) and transversely (H; thick arrow). The architecture of the RS 4% wt scaffold has not been altered even after 90 days (C, F, I). The pores (free spaces between the regenerated matrixes (I, arrows) are still present. Some of the pores have been filled with the newly regenerated tissue (N.R.T.) but some others are still free of any regeneration. Scale bar: A to C: 125 μm, D to F: 50 μm, G to I: 25 μm. *Color staining: H&E.*
RS: regenerated silk; RSF: regenerated fibroin/ silk fiber composite scaffolds.

matrix originating from the capsule started to fill the scaffold at periphery. At 90 days post implantation, the capsule thickness increased and some parts integrated within the newly regenerated tissue inside the scaffold. Through the course of the experiment, between days 30 to 90, the architecture of the scaffold was completely preserved but at long term, only a few evidences of regeneration were seen suggesting the scaffold has low biocompatibility and almost no biodegradability with minimum regenerative capacity in C57BL/6 mice. Unlike the RS 2% wt scaffolds, the RSF 2% wt scaffolds showed a similar pattern with RSF 2% wt scaffolds implanted in nude mice so that, 30 days post implantation, the RS matrix of the scaffold was almost completely degraded and replaced by the new connective tissue. Only their diameter slightly decreased by passing time. The covering capsule was well integrated with the connective tissue that regenerated inside the scaffold. At long-term follow-up, only few amounts of capsule were detected and the capsule mostly incorporated with the scaffold. In a comparative evaluation, the RSF 2% wt scaffold exhibited higher percentage of filled pores and significantly lower number of the remained pores compared to the RS 2% wt scaffolds at different time points ($P = 0.001$ for all). In addition, the RSF2% wt scaffolds had significantly higher number of fibroblast, fibrocyte and total vessels and lower number of macrophages compared to the RS 2% wt scaffolds ($P = 0.001$ for all) (Table 2).

The protein and mRNA expression of inflammatory factors in implanted scaffolds

Immunofluorescent staining of inflammatory factor "COX-2" showed a downward manner of this marker expression during three months post implantation of

Table 2. Histopathologic characteristics of various scaffolds after one to three month of subcutaneous implantation in normal and nude mice.

Animal type	Athymic nude									C57BL/6 mice					
Scaffold type	RS 4% wt			RS 2% wt			RSF 2% wt			RS 2% wt			RSF 2% wt		
Month	1	2	3	1	2	3	1	2	3	1	2	3	1	2	3
Filled pores/total pores (%)	ND	58.4 ± 10.71	59.6 ± 8.59	ND	ND	85.8 ± 5.76	ND	87 ± 6.78	83 ± 5.78	29.4 ± 10.06	32 ± 10.29	48.8 ± 4.6	71.4 ± 5.63	81.2 ± 4.81	84.8 ± 6.14
Remained pores (n)		75.4 ± 24.31	73.8 ± 14.49			21.8 ± 7.04		3 ± 2.73	3.2 ± 1.64	36.2 ± 6.79	34.4 ± 6.65	32 ± 5.24	6.6 ± 2.5	2.4 ± 2.07	2.4 ± 2.88
Total cellularity (n)		332.2 ± 37.95	808.6 ± 112.79			405.2 ± 38.52		504.2 ± 70.86	406.4 ± 26.04	675 ± 58.39	848.6 ± 96.11	277.6 ± 38.13	571.6 ± 71.75	427.4 ± 64.1	390.4 ± 18.84
Fibroblast (n)		64 ± 10.34	70.4 ± 8.44			52.4 ± 12.34		389.8 ± 25.85	282.8 ± 31.31	151.4 ± 8.44	233.2 ± 28.92	83.4 ± 12.44	361 ± 58.11	261 ± 34.09	188.4 ± 27.59
Fibrocyte (n)		21.8 ± 8.04	25.6 ± 6.38			21.2 ± 3.19		46 ± 7.31	80.4 ± 10.01	32.2 ± 6.37	93.2 ± 20.93	25.6 ± 6.69	28.4 ± 4.15	80.8 ± 11.9	98.6 ± 11.76
Lymphocyte (n)		13.2 ± 5.93	52 ± 12.84			7 ± 2.73		18.8 ± 5.81	10.6 ± 5.36	40.4 ± 12.23	15 ± 5.24	15.8 ± 6.01	29 ± 4.3	12 ± 4.41	6.6 ± 5.41
Neutrophil (n)		0.6 ± 0.54	9.2 ± 6.22			0.4 ± 0.54		0.4 ± 0.89	0	4.4 ± 4.27	1.2 ± 1.3	0	1.6 ± 1.51	0.6 ± 0.89	0
Macrophage (n)		257 ± 38.96	723.6 ± 87.25			269.6 ± 45.45		60.2 ± 13.91	41 ± 14.37	410.4 ± 44.59	500.4 ± 29.21	119.4 ± 18.94	184 ± 13.47	108.2 ± 14.34	95 ± 12.76
Small vessels (n)		2 ± 1.58	14.6 ± 2.88			12.6 ± 3.97		4.4 ± 2.07	4.2 ± 0.83	5 ± 1.22	3.6 ± 2.5	3 ± 2.12	9.8 ± 3.42	3.8 ± 1.09	3 ± 2.44
Medium vessels (n)		0	3 ± 1			1.48		0	1.2 ± 0.83	0	0	0	0	0	0
Large vessels (n)		0	2.8			1.2 ± 0.83		0.2 ± 0.44	1.2 ± 0.83	0	0	0	0	0	0

n = histopathologic field = 5, Counting magnification = ×100. Adobe Photoshop CC and Image J were used for cell and other tissue structure counting. The results are expressed as Mean ± Standard deviation. One way ANOVA with its subsequent post hoc Tukey test was used to statistically test the results and $P < 0.05$ was considered statistically significant.

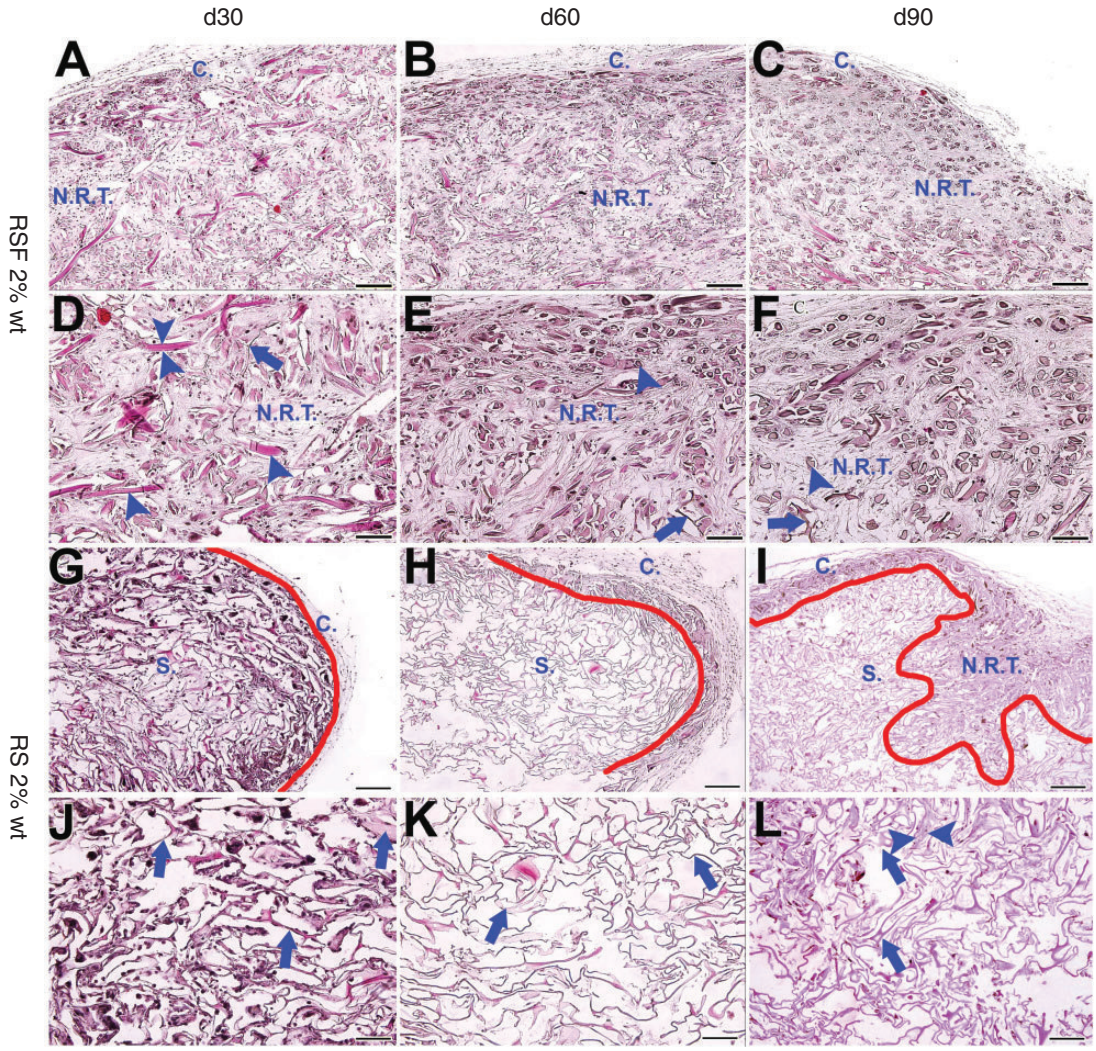

Figure 5. Histological appearance of RSF and RS 2% wt post subcutaneous implantation in C57BL/6 mice. After subcutaneous implantation of the RSF 2% wt in C57BL/6 mice (A to F), the RS matrix was almost degraded and replaced by the newly regenerated tissue (N.R.T.). The connective tissue like capsule has covered the scaffold but also it has integrated with the new matrix within the scaffold. The natural fibers are still present even 90 days post implantation so that the longitudinally (D; arrow head) and transversely (E, F: arrow head) sectioned fibers could be seen at all-time points. Few remnants of the regenerated silk matrix could be seen (E, F: arrow). After implantation of the RS 2% wt scaffold, a new capsular tissue has covered the scaffold at 30 days post implantation while time dependently its thickness has increased so that on day 90, it has invaded inside the scaffold. The newly regenerated tissue has been originated from the covering capsule and is indicated by red line (G, H, I). On day 30, only few inflammatory cells have infiltrated the scaffold (J). These cells have been apoptozed or dead due to their lifespan (K) so that the internal parts of the scaffold are free of any regenerative evidence (K). On day 90, some regenerative evidences (L; between arrows head) could be seen inside the scaffold but still most parts of the scaffold are free (L). No evidence of degradation could be seen so that the regenerated matrix (J, K, L; arrows) is almost present at all-time points. Scale bar: A to C and G to I: 125 μm; D to F; J to L 50 μm. *Color staining: H&E.*
RS: regenerated silk; RSF: regenerated fibroin/ silk fiber composite scaffolds.

the RSF 2% wt in the C57BL/6 mice (Figure 8(a)). Moreover, the mRNA expression of IL-6, COX-2 and TNF-α was assessed 30 and 90 days post implantation. As shown in Figure 8(b), although the implanted RSF 2% wt scaffolds in the C57BL/6 mice expressed IL-6 and COX-2 mRNA 30 days after transplantation, the mRNA expression of these markers down regulated 90 days post implantation; however, there were no significant differences between the TNF-α mRNA expression of the tissues retrieved at 30 and 90 days post-implantation.

Discussion

Developing an appropriate scaffold, which can provide mechanical, physical and biological support and guide

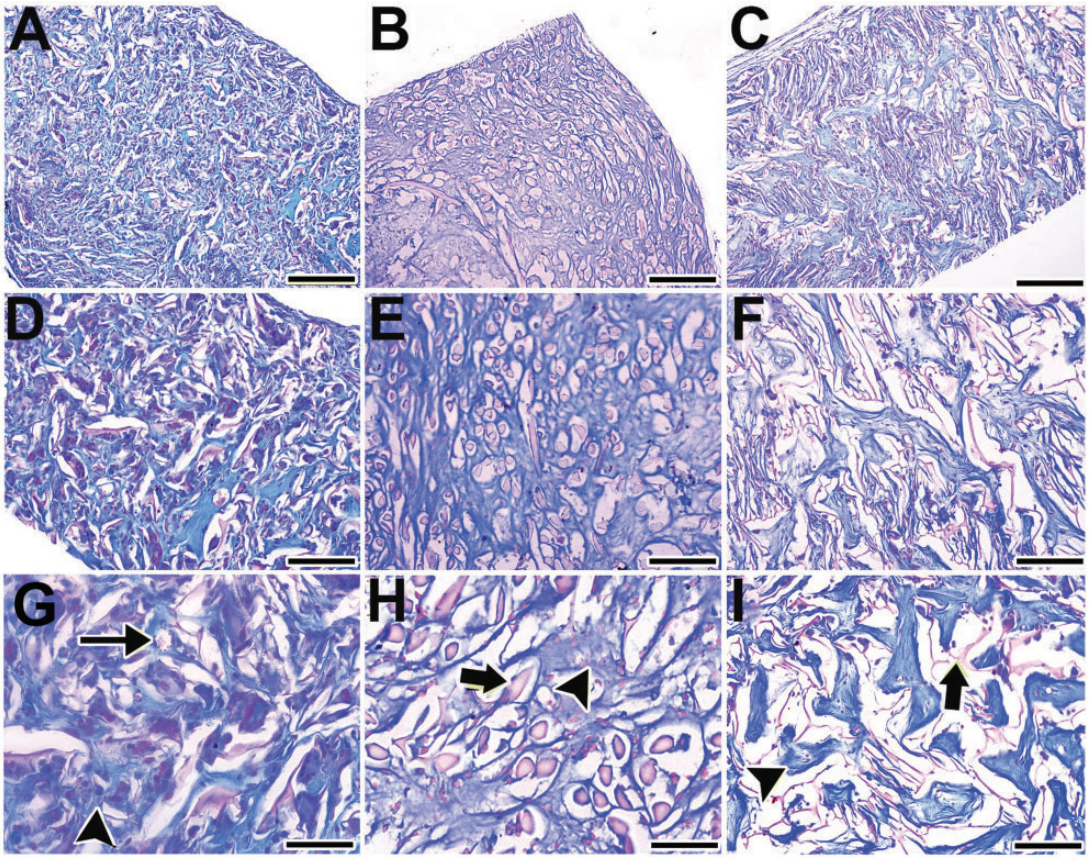

Figure 6. Alcian Blue staining of subcutaneously implanted scaffolds, 90 days post implantation in nude mice. (A, D and G) regenerated Silk (RS) 2% wt group; (B, E and H): RSF 2% wt; (C, F, I) RS 4% wt. Note the newly regenerated matrix has been stained blue while the cellular structures and the scaffold has been stained red. The RS 2% wt scaffold has not been degraded by the host, but the newly regenerated tissue has well filled the free spaces of the scaffold and the free pores. In contrast to the RS 2%, the RSF 2% scaffold has been almost completely degraded but the natural fibers are still present (H; thick arrow). The newly regenerated matrix (H; arrow head) has well filled the free spaces of the scaffold and covered the fibers. In the RS 4% group, less matrix has regenerated inside the scaffold, the architecture (I, arrow) of the scaffold is still preserved and more free spaces in the scaffold could be seen. Scale bar: A to C: 50 μm; D to F: 25 μm; G to I: 12.5 μm. Stained with AB/NFRS.

cell growth to the new tissue, is essential aspect in osteochondral tissue engineering.[25] Fiber-reinforced scaffolds have been in the focus of the attention due to the presence of suitable mechanical properties along with proper porosity.[26] We showed that embedding natural silk fibers in the RS matrix would be able to increase the young modulus of the 2 wt% RS scaffolds up to ten folds (13.97 MPa), while the porosity of the scaffolds are almost the same. This improvement is due to transferring the mechanical loads to the fibers which originally have superior mechanical properties than the RS matrix.[17] In addition to appropriate physical and mechanical properties, in preliminary part of this study, we showed that this RS scaffold mediates suitable matrix for attachment, homing and proliferation of BMSCs recommending it as a good candidate for reconstruction of osteochondral tissues. Subsequently, we have evaluated the *in vivo* behavior of subcutaneously implanted RS and RSF scaffolds to figure out the effect of embedded fibers in the composite construct on biodegradation and tissue regeneration during three months in mice. Subcutaneous model was considered for the *in vivo* study based on the ease of the implantation surgery and the need to evaluate biodegradation and biocompatibility of scaffolds in vascular tissues.[16–19] We demonstrated that the RSF 2% wt scaffolds are biocompatible, partially biodegradable and have superior regenerative properties compared to those of the RS 2 and 4% wt ones.

Biodegradability of an tissue engineered construct is an important factor for development of a newly regenerated tissue in the shortest possible time.[16,27,28] Low biodegradability of the natural silk fibers has been endorsed by showing long-term degradation of at least 6 to 24 months by the host immune system (Table 3). *In vitro* and *in vivo* investigations regarding the RS fibroin have shown that aqueous-derived scaffolds degrade quicker with less immune system reaction

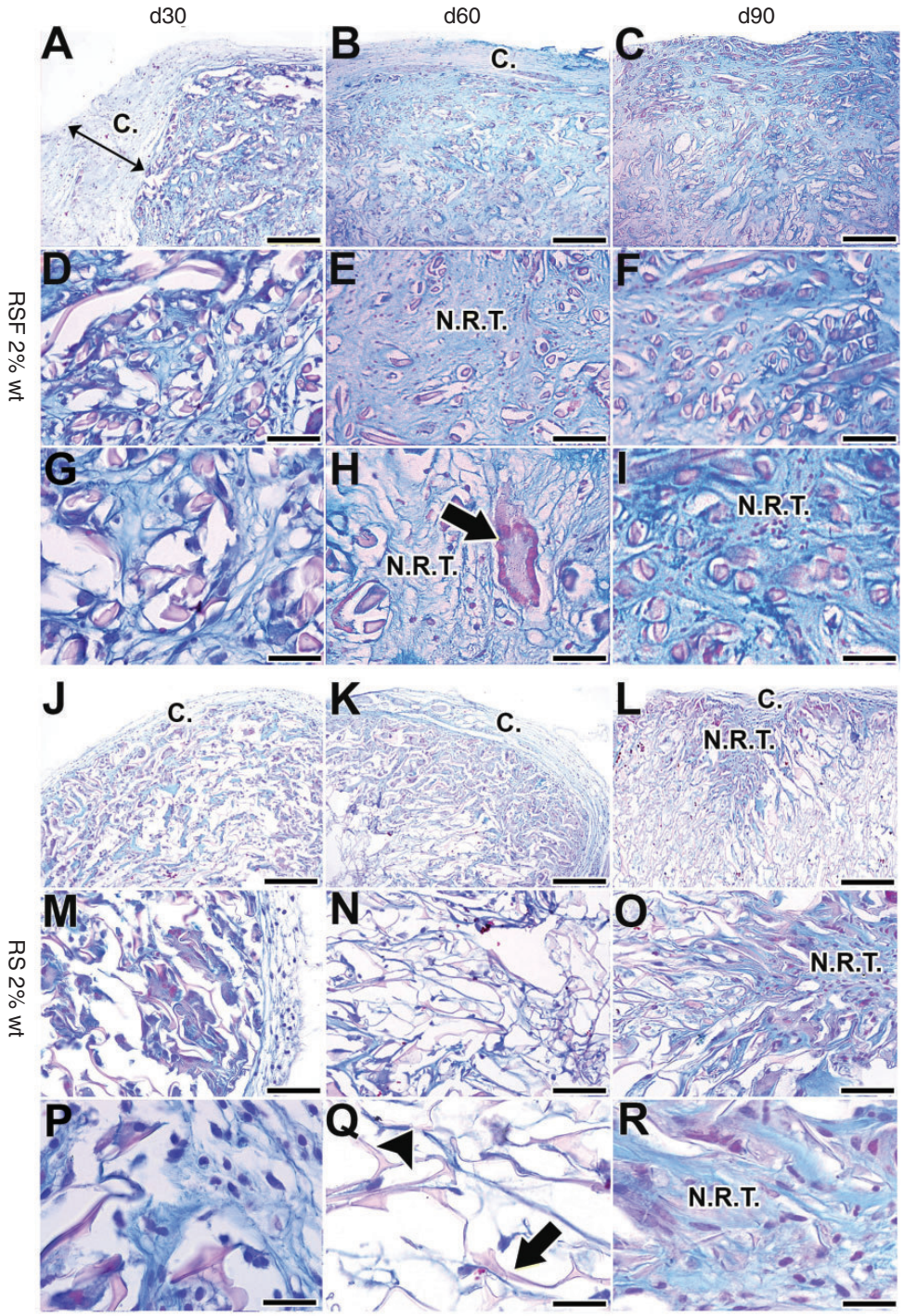

Figure 7. Alcian Blue staining of subcutaneously implanted scaffolds in C57BL/6 mice. In the RSF 2% scaffolds, a thick capsule (c) has covered the scaffold at 30 days post implantation (A; Arrows). By passing time from day 30 to 90, the thickness of the capsule has been decreased so that at 90 days (C), the capsule has completely merged with the scaffold. In the RSF group, most of the regenerated Silk matrix has been degraded and replaced by the newly regenerated tissue (N.R.T.), large and matured blood vessels have filled the internal parts of the scaffold (H; arrow), the natural fibers have not been degraded but time dependently the density of the newly regenerated tissue (N.R.T.) has been increased. In the RS 2% wt scaffold, a loose capsule (c) has covered the scaffold but its thickness has been increased, time dependently. The architecture of the scaffold has been completely preserved by the host. At mid to long-term follow-up, few matrix (Q, arrow head) has infiltrated the free pores of the scaffold (Q, arrow). Scale bar: A to C, J to L; 125 μm; D to F, M to O; 50 μm; G to I and P to R; 25 μm. (Stained with AB/NFR).
RS: regenerated silk; RSF: regenerated fibroin/ silk fiber composite scaffolds.

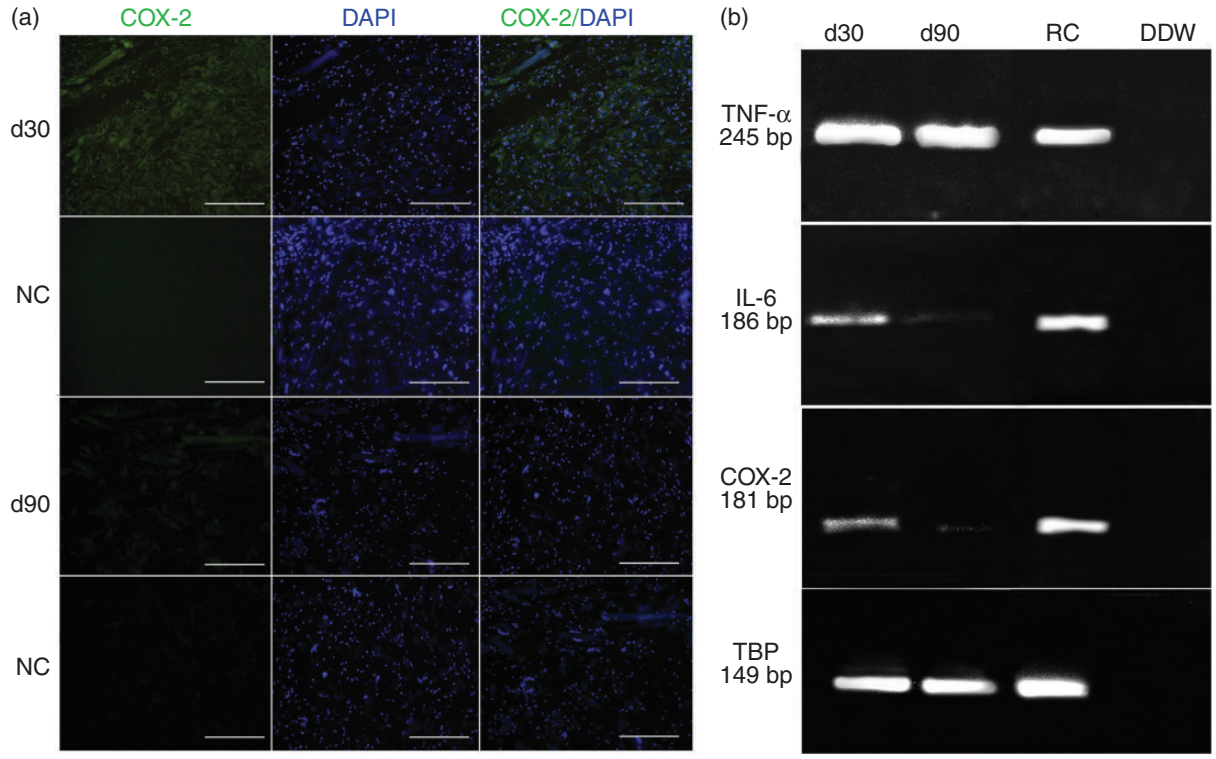

Figure 8. Immunofluorescent staining and RT-PCR. (a) The expression of COX-2 protein was evaluated in the RSF 2% wt scaffold, 30 and 90 days post subcutaneous implantation in mice. Negative controls (NC) included rabbit IgG substitution of primary antibody. Samples have been incubated with DAPI (1:1000) for nuclear staining. Scale bar: 500 μm (b) RT-PCR; Gene expression of the inflammatory markers (TNF-α, IL-6 and COX-2) in the RSF 2% wt scaffolds, 60 and 90 days post subcutaneous implantation in C57BL/6 mice. TBP, RAW264.7 (mouse leukemic monocyte macrophage cell line; RC) and D.D.W. have been used as internal, positive and negative controls, correspondingly.
TNF-α: Tumor necrosis factor-α; COX-2: cyclooxygenase-2; IL-6: interleukin-6; TBP: TATAA-box binding protein.

in comparison with organic solvent-derived scaffolds.[16,29–31] However, based on the knowledge of the authors, there is no systematic study reported the degradation behavior of degummed silk fibers *in vivo*. In the present study, the *in vivo* degradation of degummed silk fibers in combination with aqueous-derived RS fibroin was investigated.

We showed that it is possible to improve the biocompatibility, biodegradability and regenerative capacity of silk-based scaffolds by two-step optimization including decrease in the concentration of the RS matrix and assembling the matrix with the natural degummed silk fibers.

Based on the findings of the present study, although natural silk fibers had low *in vivo* biodegradability in both nude and C57BL/6 mice, the RS matrix was completely degraded and replaced by the newly developed connective tissue through embedding the natural fibers within the matrix, suggesting the natural silk fibers may have a role in increasing the biodegradability of the RS matrix. It seems that the natural silk fibers probably boost the degradation of the regenerated matrix due to a slight rise in initial foreign body reaction. These data may emphasize the ability of these fibers in escalating the specific surface area, which results in increasing the number of immigrated cells within the RS matrix. The superior cellular infiltration response observed in the RSF 2% wt scaffolds compared to those of the RS 2 and 4 % wt ones, confirmed the above theory. A robust evidence for this assumption was lower degradation rate of the RS 4% with smaller pore size and subsequently less cell infiltration compared to those of the RS 2% and RSF 2% ones with larger pore size and higher cell infiltration level.

Another important characterization of a construct is its biocompatibility, endorsing the ability of a construct to be tolerated by the host immune response.[5] Based on our results, the degradation behavior of RSF 2% wt scaffolds in nude mice is superior compared to that of the RS 2 and 4% wt ones. Moreover, the higher areas of newly developed interconnected well-differentiated matrix was observed in RSF 2% wt constructs suggesting that embedding the natural fibers within the regenerated matrix has a considerable value in increasing the biocompatibility of the construct. Unlike RSF 2% wt, high infiltration of immune cells long term post

Table 3. Degradation of *B. Mori* Silk, *in vivo* and *in vitro* studies.

		In vitro study			*In vivo* study			
Silk-based material	Pore Size (μm)	Degradation degree	Conditions	Duration	Degradation degree	In vivo model	Duration	Reference
8% wt-aqueous derived	~850	30% reduce in surface area	PBS −37°C	56 days	–	–	–	(Park et al.[29])
8% wt- organic solvent HFIP (hexafluoro-2-isopropanol)	~850	9% reduce in surface area	PBS −37°C	56 days	–	–	–	(Park et al.[29])
1% wt fibroin + 3% wt chitosan	100–150	18% mass loss	PBS −37°C	60 days	–	–	–	(Zhu et al.[23])
Degummed silkfiber scaffolds	Mesh	~ 3% mass loss	PBS −37°C	42 days	–	–	–	(Horan et al.[30])
Degummed silkfiber scaffolds	Mesh	50% mass loss	PBS −37°C+ protease XIV (1 mg/ml)	42 days	–	–	–	(Horan et al.[30])
Degummed silkfiber scaffolds	Mesh	25% mass loss	PBS −37°C+ protease XXIII (1 mg/ml)	10 weeks	–	–	–	(Srihanam and Simchuer[31])
6% wt aqueous derived	850–1000	–	–	–	100%	Lewis rat/ subcutaneously	24 weeks	(Wang et al.[8])
10% wt aqueous derived	850–1000	–	–	–	~67%	Lewis rat/ subcutaneously	24 weeks	(Wang et al.[8])
6% wt organic solvent HFIP (hexafluoro-2-isopropanol)	850–1000				~0%	Lewis rat/ subcutaneously	1 year	(Wang et al.[8])

PBS: phosphate-buffered saline.

implantation in nude mice narrates low biocompatibility of the RS 4 % wt scaffold.

Regenerative capacity is another necessary concept for the identification of *in vivo* efficacy of tissue-engineered scaffolds. There are several factors that determine the regenerative capability of a scaffold including scaffold porosity, pore size and morphology, biodegradation profile and biocompatibility.[32,33] Based on the results observed in the nude mice, the RS 2% wt and RSF 2% wt scaffolds exhibited superior regenerative properties than those of the RS 4% wt ones. Unlike those of the 4% wt scaffolds, the architecture of the RS 2% wt ones was partially replaced by the new tissue. The tissue almost completely expanded throughout the scaffold and no islands of regenerated tissue were similar to those observed in the 4% ones so that the regenerated tissue in the RS 2% wt scaffold showed more homogeneity. Embedding the natural non-degradable silk fibers within the regenerated matrix increased the regenerative properties of the scaffold so that more homogenous newly regenerated tissue with a denser structure had formed in the RSF 2% wt scaffolds compared to those of the RS 2 and 4 % wt ones.

Undesirable regenerative properties of RS 4% wt may be attributed to the low biodegradability of this construct inhibiting the connection between regenerated matrices to establish.

With retrieving the primary data regarding differences between different silk-based scaffolds in nude mice, we cancelled the study of RS 4% wt scaffold and investigated behavior of the RS 2% wt and RSF 2% wt scaffolds in C57BL/6 mice subsequently. These following investigations were settled to more assessment of biodegradation, biocompatibility and regenerative properties of RSF2% wt scaffold in a wild type instead of athymic nude animal. Based on our results, although implantation of the RS 2% wt scaffold in nude mice suggested the biocompatibility of the scaffold, subcutaneous implantation of the RS 2% wt scaffold in the C57BL/6 mice resulted in a different judgment. In fact, after subcutaneous implantation of the RS 2% scaffold in C57BL/6 mice, few inflammatory cells infiltrated in the internal parts of the scaffold at 30 days post implantation, while at 60 days almost no cell was seen inside the scaffold suggesting the cells were dead due to their life span. In a similar manner with nude mice, the regenerative capability of the scaffolds in the C57BL/6 mice judged by degradation of the RS matrix by the host and the matrix replacement by the more homogenous new tissue was significantly higher in RSF 2% wt compared to RS 2% wt scaffolds. While after three months, low tissue ingrowths developed in the RS 2% wt scaffolds, this characteristic was observed in the RSF 2% only after 30 days of implantation. Following these results, the biocompatibility of RSF 2% wt scaffolds was more confirmed by assessment of inflammatory factors like COX-2, IL-6 and TNF-α. Initial immune response judged by expression of COX-2 and IL-6 could be attributed to better cellular access due to the presence of fibers and angiogenesis which accelerates degradation.[16] However, this early inflammation subsided over the time. Although COX-2 and IL-6 factors were time-dependently down-regulated, TNF-α showed no significant changes. Based on the available reports showing an important physiological role of TNF-α in regulating skeletal muscle regeneration,[34] it seems that the expression of the TNF-α in the RSF 2% wt scaffolds, even after 90 days, probably had improving effects on the regeneration.

Based on these data, although biodegradation time of silk fibers are much more than other natural polymers like collagen (4–12 weeks),[35,36] embedding the natural degummed silk fibers within the RS matrix is a novel technology that shortens biodegradation time of silk-based scaffolds. The newly regenerated tissue replaced the RS matrix, was a non-aligned tissue and this was due to the porous structure of the scaffold, which we have shown in our *in vitro* results.[17,20] Such a construct with the numerated and well discussed characteristics may be a suitable option in bone and or cartilage tissue engineering purposes because both these structures have bulky architecture and the matrix is not aligned in these tissues.[8] However, more studies are needed to elucidate its beneficial effects on the healing and regeneration of injured bone or cartilage.

Conclusion

This study investigated *in vivo* biodegradability and biocompatibility of the regenerated silk scaffolds, which reinforced with natural degummed silk fibers. The results showed that the presence of degummed silk fibers in the composite scaffolds, significantly enhances the mechanical compressive properties to more than 10 folds compared to those without natural fiber. Moreover, the biocompatibility, biodegradability and regenerative properties were observed in the reinforced scaffolds were more typical when compared to controls. These outcomes demonstrated that embedding the silk fibers within the matrix enhances the biodegradability of the matrix through giving a rise in specific surface area of scaffolds and resulting in almost complete replacement of the scaffolds with the fresh connective tissue. The findings of the present study indicate the key role of the embedded fibers in improving the mechanical and biological properties of the silk-based scaffolds and suggest the potential ability

of the presented scaffold for connective tissue regeneration especially osteochondral defects.

Acknowledgements

The authors would like to thank the authorities of Avicenna Research Institute for their financial supports and providing facilities to perform this research. The authors would like to thank Zahra Ghaempanah and Maryam Rahimi for their assistance in lab works; Mohammad Ebrahim Sohrabi for preparing histo-pathologic sections; Morteza Gholizadeh-Farab and Farhad Hosseini for helping in animal surgeries.

Authors' contributions

SM and MT-J contributed equally in this work.

Declaration of Conflicting Interests

The author(s) declared no potential conflicts of interest with respect to the research, authorship, and/or publication of this article.

Funding

The author(s) disclosed receipt of the following financial support for the research, authorship, and/or publication of this article: Avicenna Research Institute, ACECR, Tehran, Iran supported this study (Grant Number: 19380).

References

1. Burg KJ, Porter S and Kellam JF. Biomaterial developments for bone tissue engineering. *Biomaterials* 2000; 21: 2347–2359.
2. Cancedda R, Dozin B, Giannoni P, et al. Tissue engineering and cell therapy of cartilage and bone. *Matrix Biol* 2003; 22: 81–91.
3. Griffith LG and Naughton G. Tissue engineering current challenges and expanding opportunities. *Science* 2002; 295: 1009–1014.
4. Hutmacher DW, Schantz JT, Lam CX, et al. State of the art and future directions of scaffold-based bone engineering from a biomaterials perspective. *J Tissue Eng Regen Med* 2007; 1: 245–260.
5. Hutmacher DW. Scaffolds in tissue engineering bone and cartilage. *Biomaterials* 2000; 21: 2529–2543.
6. Altman GH, Diaz F, Jakuba C, et al. Silk-based biomaterials. *Biomaterials* 2003; 24: 401–416.
7. Vepari C and Kaplan DL. Silk as a biomaterial. *Prog Polym Sci* 2007; 32: 991–1007.
8. Wang Y, Kim HJ, Vunjak-Novakovic G, et al. Stem cell-based tissue engineering with silk biomaterials. *Biomaterials* 2006; 27: 6064–6082.
9. Hardy JG, Römer LM and Scheibel TR. Polymeric materials based on silk proteins. *Polymer* 2008; 49: 4309–4327.
10. Hardy JG and Scheibel TR. Composite materials based on silk proteins. *Prog Polym Sci* 2010; 35: 1093–1115.
11. Rahimi M, Zarnani AH, Mohseni-Kouchesfehani H, et al. evaluation of cardiac markers in differentiated cells from menstrual blood and bone marrow-derived-stem cells in vitro. *Mol Biotechnol* 2014; 56: 1151–1162.
12. Freed LE, Vunjak-Novakovic G, Biron RJ, et al. Biodegradable polymer scaffolds for tissue engineering. *Biotechnology* 1994; 12: 689–693.
13. Sung H-J, Meredith C, Johnson C, et al. The effect of scaffold degradation rate on three-dimensional cell growth and angiogenesis. *Biomaterials* 2004; 25: 5735–5742.
14. Cao Y and Wang B. Biodegradation of silk biomaterials. *Int J Mol Sci* 2009; 10: 1514–1524.
15. Horan RL, Antle K, Collette AL, et al. In vitro degradation of silk fibroin. *Biomaterials* 2005; 26: 3385–3393.
16. Wang Y, Rudym DD, Walsh A, et al. In vivo degradation of three-dimensional silk fibroin scaffolds. *Biomaterials* 2008; 29: 3415–3428.
17. Mobini S, Hoyer B, Solati-Hashjin M, et al. Fabrication and characterization of regenerated silk scaffolds reinforced with natural Silk fibers for bone tissue engineering. *J Biomed Mater Res Part A* 2013; 101: 2392–2404.
18. Liu X, Rahaman MN, Hilmas GE, et al. Mechanical properties of bioactive glass (13-93) scaffolds fabricated by robotic deposition for structural bone repair. *Acta Biomater* 2013; 9: 7025–7034.
19. Gogolewski S, Jovanovic M, Perren SM, et al. Tissue response and in vivo degradation of selected polyhydroxyacids: polylactides (PLA), poly(3-hydroxybutyrate) (PHB), and poly(3-hydroxybutyrate-co-3-hydroxyvalerate) (PHB/VA). *J Biomed Mater Res* 1993; 27: 1135–1148.
20. Mobini S, Solati-Hashjin M, Peirovi H, et al. Bioactivity and biocompatibility studies on silk-based scaffold for bone tissue engineering. *J Med Biol Eng* 2013; 33: 207–213.
21. Kim U-J, Park J, Joo Kim H, et al. Three-dimensional aqueous-derived biomaterial scaffolds from silk fibroin. *Biomaterials* 2005; 26: 2775–2785.
22. Kweon H and Park YH. Dissolution and characterization of regenerated antheraea pernyi silk fibroin. *J Appl Polym Sci* 2001; 82: 750–758.
23. Zhu Z, Ohgo K and Asakura T. Preparation and characterization of regenerated Bombyx mori Silk fibroin fiber with high strength. *eXPRESS Polym Lett* 2008; 2: 885–889.
24. Kazemnejad S, Allameh A, Soleimani M, et al. Biochemical and molecular characterization of hepatocyte-like cells derived from human bone marrow mesenchymal stem cells on a novel three-dimensional biocompatible nanofibrous scaffold. *J Gastroenterol Hepatol* 2009; 24: 278–287.
25. Chung C and Burdick JA. Engineering cartilage tissue. *Adv Drug Deliv Rev* 2008; 60: 243–262.
26. Li X, Yang Y, Fan Y, et al. Biocomposites reinforced by fibers or tubes as scaffolds for tissue engineering or regenerative medicine. *J Biomed Mater Res Part A* 2014; 102: 1580–1589.
27. Rezwan K, Chen Q, Blaker J, et al. Biodegradable and bioactive porous polymer/inorganic composite scaffolds for bone tissue engineering. *Biomaterials* 2006; 27: 3413–3431.

28. Moshiri A, Oryan A and Meimandi-Parizi A. Role of tissue-engineered artificialtendon in healing of a large Achilles tendon defect model in rabbits. *J Am Coll Surg* 2013; 217: 421–441.
29. Park S-H, Gil ES, Shi H, et al. Relationships between degradability of Silk scaffolds and osteogenesis. *Biomaterials* 2010; 31: 6162–6172.
30. Horan RL, Antle K, Collette AL, et al. In vitro degradation of Silk fibroin. *Biomaterials* 2005; 26: 3385–3393.
31. Srihanam P and Simchuer W. Proteolytic degradation of Silk fibroin scaffold by protease XXIII. *Open Macromol J* 2009; 3: 1–5.
32. Hollister SJ. Porous scaffold design for tissue engineering. *Nature Mater* 2005; 4: 518–524.
33. Oryan A, Moshiri A, Parizi AM, et al. Implantation of a novel biologic and hybridized tissue engineered bioimplant in large tendon defect: an in vivo investigation. *Tissue Eng Part A* 2014; 20: 447–465.
34. Chen S-E, Gerken E, Zhang Y, et al. Role of TNF-α signaling in regeneration of cardiotoxin-injured muscle. *Am J Physiol Cell Physiol* 2005; 289: C1179.
35. Rothamel D1, Benner M, Fienitz T, et al. Biodegradation pattern and tissue integration of native and cross-linked porcine collagen soft tissue augmentation matrices – an experimental study in the rat. *Head Face Med* 2014; 10: 10.
36. Owens KW and Yukna RA. Collagen membrane resorption in dogs: a comparative study. *Implant Dent* 2001; 10: 49–58.